Electron-momentum spectroscopy of fullerene

M. Vos,* S. A. Canney, I. E. McCarthy, and S. Utteridge
Electronic Structure of Materials Centre, Flinders University of South Australia, GPO Box 2100, Adelaide 5001, Australia

M. T. Michalewicz
CSIRO Mathematical and Information Sciences, Swanston Street, Carlton, Victoria 3053, Australia

E. Weigold
Research School of Physical Sciences and Engineering, Institute of Advanced Studies, The Australian National University, Canberra 0200, Australia

(Received 7 January 1997)

The energy-resolved electron-momentum density of fullerene has been measured. Clear differences are found from the energy-momentum densities of either diamond or graphite. The energy-momentum density of fullerene can be described as being composed of a σ band and a split π band. The observed spectral momentum densities are compared to the calculated orbitals of a C_{60} molecule in momentum space. Good agreement is found. A simple classification of the orbitals is proposed that explains elegantly the calculated and observed structures. The splitting of the π band can be interpreted as a consequence of the curvature of the carbon network forming the fullerene molecule. [S0163-1829(97)01927-9]

I. INTRODUCTION

Carbon is an element that can form solids with an extremely wide range of properties. The graphite and diamond forms have been studied for a long time. These represent the prototypical example of how two solids, made from the same element, can have completely different properties. Somewhat more recent is the study of its amorphous forms. Depending on its preparation one can have again solids with properties ranging from diamondlike to graphitelike.[1] More recently carbon was discovered to occur in other forms, firstly fullerene, a large, highly symmetrical molecule. For a review of many of its properties see Dresselhaus *et al.*[2]

The different properties are a consequence of the different geometrical structure, that lead to different forms of bonding between the valence electrons. A very direct way of observing the valence electron structure is electron-momentum spectroscopy (EMS) [also called $(e,2e)$ spectroscopy]. It measures the spectral momentum density of occupied states, i.e., the probability that an electron with binding energy ε has momentum $\mathbf{q}$. It has been used to study a wide variety of carbon films, from well-ordered single crystal graphite,[3] highly oriented pyrolitic graphite[4] to highly disordered forms of diamondlike[5] and graphitic amorphous carbons.[6] In this paper we extend these studies to films of fullerite (solid C_{60}).

Fullerite is closer to graphite than diamond. Each carbon atom in C_{60} is bonded to three other carbon atoms by two types of bonds with lengths 1.45 Å and 1.40 Å. In graphite each atom is bonded to its three neighbors (bond length 1.42 Å). The shortest distance between atoms of different molecules in fullerite is slightly less than the interplanar distance in graphite (3.18 Å versus 3.45 Å). In diamond, however, each carbon atom is bonded to four neighbors, with a larger bond length of 1.54 Å.

As the fullerene molecules form only weak intramolecular bonds, we expect that within the limited energy resolution of the present EMS studies ($\simeq$0.9 eV) the measured spectral momentum densities will be well described as the sum of the spectral momentum densities of independent molecules. Indeed calculated dispersion of the energy band associated with the highest occupied molecular orbital (HOMO) in a C_{60} solid is of the order of 0.5–0.8 eV. Further the fullerene molecules will be randomly oriented in our room-temperature experiment, so our intensity will be proportional to the spherically averaged spectral momentum density of a C_{60} molecule. Since C_{60} is a highly spherical molecule this angular averaging affects the measurement only in a minor way.

II. ELECTRON-MOMENTUM SPECTROSCOPY

If a beam of high-energy electrons strikes a target, some of these electrons will scatter from target electrons. For ionizing collisions the energy and momentum transferred by the impinging electron ejects a target electron. EMS or $(e,2e)$ spectroscopy, as described here, involves collisions with large momentum transfer which allows us to describe the collision between impinging and target electrons as a *binary* collision.[7]

The label $\mathbf{p}$ will denote electron momenta as determined outside a molecule or crystal and $\mathbf{q}$ the real momentum of the electron to be ejected in the molecule or crystal immediately *before* the scattering event. The scattered and ejected electrons are detected *in coincidence* and analyzed for their energies and momenta (E_s and $\mathbf{p}_s$ for the slower of the two electrons, E_f and $\mathbf{p}_f$ for the faster one).

Comparing the momenta and energies of the scattered and ejected electrons with the momentum $\mathbf{p}_0$ and energy E_0 of the incident electron yields the magnitudes of the momentum and binding energy of the ejected electron *before* the collision. We thus determine the binding energy ε as

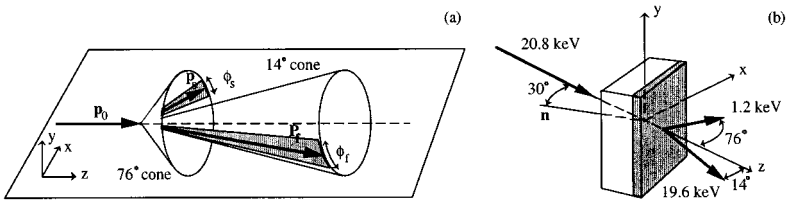

FIG. 1. Schematic representation of the geometry of the $(e,2e)$ experiments. In (a) we show the range of azimuthal angles measured and in (b) the sample orientation with respect to all three electron beams. Most structural information is obtained from the shaded area of the sample since the slow electron has the smallest mean free path.

$$\varepsilon = E_0 - E_s - E_f . \tag{1}$$

At sufficiently high energies the incoming and outgoing electrons can be treated as plane waves and the momentum of the target electron before the collision is given by

$$\mathbf{q} = \mathbf{p}_s + \mathbf{p}_f - \mathbf{p}_0 . \tag{2}$$

A complete description of the kinematics of each ionizing event is thus obtained. Moreover for high energies of the incoming and outgoing particles the measured intensity is proportional to the energy-momentum density. If we resolve a molecular level with energy ε we can associate the measured intensity $I(\varepsilon,\mathbf{q})$ directly with $|\phi_\varepsilon(\mathbf{q})|^2$, the squared modulus of the electron orbital in momentum space. If the different orbitals are not resolved then we call the measured quantity the spectral (or energy-) momentum density. This is equal to the sum of the intensity of all the orbitals involved per unit energy. This direct relation between the measured intensity and the orbital in momentum space is an outstanding property of the $(e,2e)$ technique and for this reason it is often referred to as electron momentum spectroscopy.[7]

We choose atomic units (a.u.) setting $\hbar = 1$, and thereby equating momenta and wave numbers. (One a.u. as a unit of length corresponds to 0.529 Å, 1 a.u. of momentum corresponds to 1.89 Å^{-1}.) In the present spectrometer the momentum resolution is 0.1 a.u. and the energy resolution is approximately 1 eV.

The experimental configuration of our $(e,2e)$ spectrometer is shown in Fig. 1. Achieving sufficient momentum and energy resolution requires a well-collimated monoenergetic electron beam impinging on a target. The incoming electron beam has an energy of $\simeq 20.8$ keV. The two detectors are positioned at polar angles of 14° (fast electron detector) and 75.6° (slow electron detector) with respect to the incoming beam. The energies of the detected electrons are $\simeq 19.6$ keV and $\simeq 1.2$ keV, respectively. Both detectors accept electrons emerging from the target over part of a cone around the incident beam direction (see Fig. 1, the azimuthal angular range being $\pm 10°$ for the fast electron detector, $\pm 6°$ for the slow one).[8] Under these conditions the sum of the momenta of the slow and fast electron equals the momentum of the incoming one, if all three electron trajectories (the incoming and the two outgoing ones) are in the same plane. If this is not the case then the momentum deficit $\mathbf{q}$ as calculated from Eq. (2) is directed approximately along the y axis.

Thus, if multiple scattering effects are neglected, one can associate the measured intensity with

$$I(\varepsilon,\mathbf{q}) = \sum_{\varepsilon} |\phi_\varepsilon(0,q_y,0)|^2,$$

with the sum extending over all the orbitals in the energy window involved as a consequence of the finite energy resolution. Unfortunately, for experiments on solids a significant fraction of the $(e,2e)$ events suffer from multiple scattering. Inelastic scattering (mainly plasmon creation) causes the excitation energy to be added to the binding energy inferred from Eq. (1). Elastic scattering from the atomic cores causes an additional transfer in momentum, and hence the value of $\mathbf{q}$ as inferred from Eq. (2) is not exactly equal to the momentum of the target electron. Nevertheless we can clearly observe the ''clean'' events (i.e., those without multiple scattering) as well defined features on a smooth background due to events with multiple scattering. For a quantitative analysis of multiple scattering see Ref. 9.

In these measurements we evaporate a thin C_{60} film onto a 50 Å free-standing amorphous carbon substrate. Due to the small mean free path of the slow outgoing electron we expect to get almost exclusively information on the surface layer facing the slow electron detector [the shaded area in Fig. 1(b)], in this case the C_{60} film. After the evaporation the sample was transferred under vacuum into the spectrometer. In both the preparation chamber and the spectrometer the pressure was in the low 10^{-10} torr range.

This sample preparation procedure has worked well in the past for amorphous silicon films[10] and aluminum films.[11] However, if the amorphous carbon film is not homogeneously covered by the C_{60} film it will also contribute to the spectra. Justification of the data is somewhat less straight forward in the present case than usual, as all elements involved are carbon. However, as we will see, there are strong features in the experimental spectra not seen in amorphous carbon, and these peaks are separated in energy in the same way as the peaks in the photoemission spectra of C_{60}. Thus we are confident that the spectra are at least dominated by the contributions of C_{60}.

III. CALCULATIONS

Calculations of molecular orbitals were done for isolated C_{60} molecule. In order to compute the molecular orbitals ψ_i we used a density functional theory method as implemented in the DGauss program.[12,13] DGauss is a part of *UniChem*, a suite of computational quantum chemistry programs from Cray Research, Inc. (presently maintained by Oxford Molecular).[14]

The TZ94 basis set was used at fixed geometry to compute molecular orbitals for all 120 electronic valence states. The computation was performed at the local density approximation (LDA) level which included Vosko-Wilk-Nusair local potential. The nonlocal exchange-correlation was computed after LDA self-consistently using the Becke-Stoll-

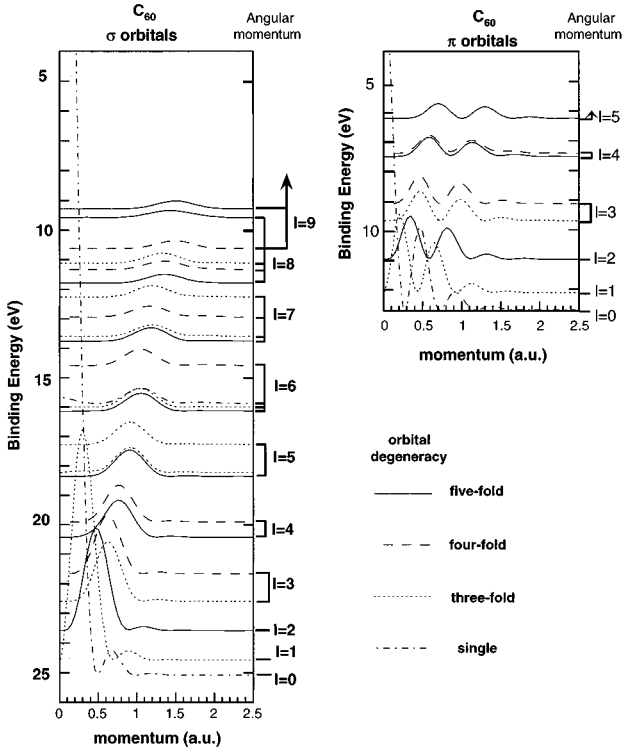

FIG. 2. The calculated spherical average of the momentum densities of each orbital in C_{60}. In (a) we show the shape of the orbitals with σ character, in (b) for those with π character. All orbitals are shifted vertically by an amount proportional to the binding energy. The different degeneracies are indicated by different line types.

Pavlidou-Preuss correction.[14] The molecular coordinates at the optimum geometry (minimized energy) were taken from Ref. 15.

For each molecular orbital we calculated the spherically averaged momentum density.[7] These are plotted in Fig. 2. Due to the large amount of symmetry, many of these orbitals are degenerate. This is indicated in the plot by different line types. (The degeneracy level indicated does not include the spin degeneracy.) The indicated binding energies are calculated for isolated molecules relative to the vacuum level.

There are in total 32 occupied levels, but it is at once obvious that there is a pattern that governs the evolution of the shape of the orbitals with decreasing binding energy. There is one group evolving from an orbital with a binding energy of 25.1 eV and maximum density at zero momentum to an orbital with a binding energy of 9.2 eV with a maximum intensity at 1.6 a.u. There are in total 180 electrons accommodated in this group. The other group extends from 12.7 eV binding energy to 6.25 eV binding energy. Again the densities peak at higher momenta with decreasing binding energy, but now there is a peculiar double-peaked structure in each of these densities. There are in total 60 electrons accommodated in the second group.

For graphite we can distinguish between two bands with different symmetries. The σ band is formed from the $2s$ and $2p_x$ and $2p_y$ atomic orbitals (the x and y directions are in the plane of the graphite), and the π band is formed by the $2p_z$ electrons. The latter is antisymmetric relative to the graphitic plane. In C_{60} this division cannot be made exactly, due to the curvature of the carbon network, but there is one set of orbitals that changes sign at an approximate sphere with a radius of about 3.55 Å. These orbitals are in many ways equivalent to the π electrons in graphite, but have some σ character mixed in as well.[16] Thus in a C_{60} molecule the first group containing 180 electrons are similar to the σ orbitals in graphite and the second group of 60 electrons resemble the π electrons.

The maximum momentum density seems to decrease with orbitals which peak at larger values of q. However the number of electrons with momenta between q and $q+\Delta q$ is proportional to $4q^2$. Our spectrometer only accepts electrons with a momentum value approximately on a straight line in momentum space. Hence it emphasizes the low momentum part of the wave function in the same way as these calculations.

IV. RESULTS

In Fig. 3 we show a plot of experimental results for a C_{60} film prepared as described. As EMS resolves both binding energy and target electron momentum, the results are contained in a two-dimensional array which we represent as a grey scale plot. The darker the shading the larger the measured intensity. In our spectrometer the natural energy reference level is the vacuum level. In the case of measurements

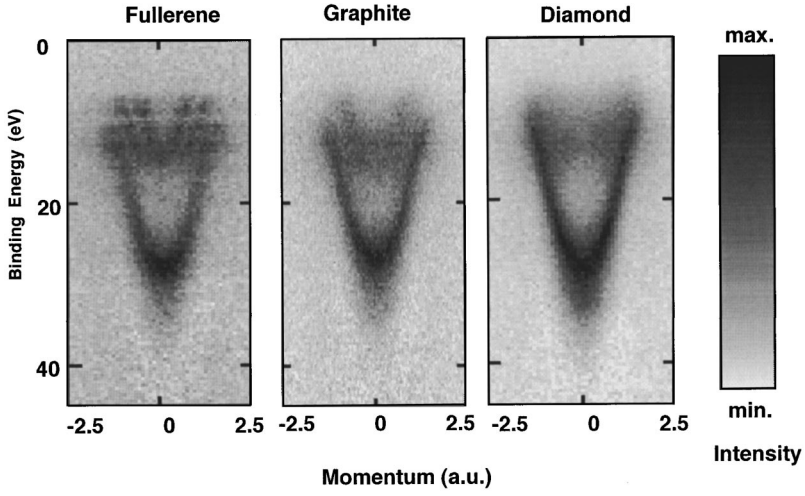

FIG. 3. The measured energy-momentum density of different forms of carbon as indicated. Note the absence of a π band in the amorphous diamond film, a single π band for polycrystalline graphite, and a double π band for fullerite.

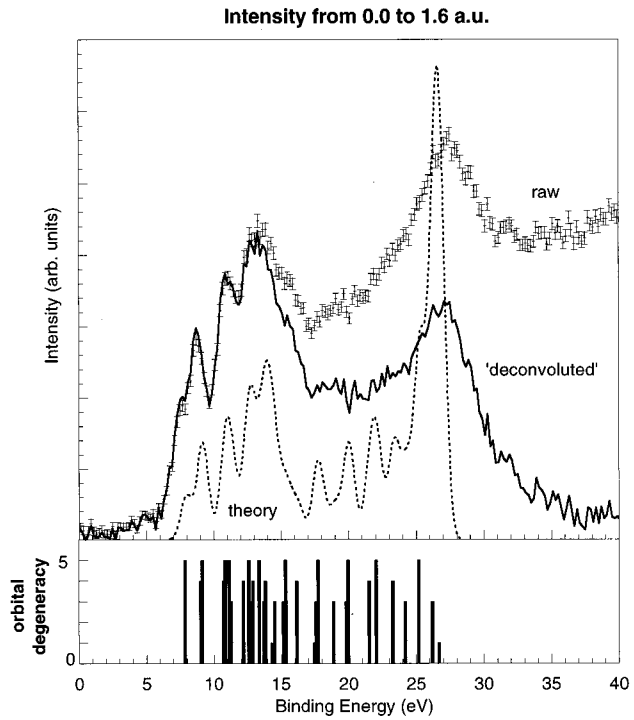

FIG. 4. The momentum integrated spectrum of a C_{60} film. Note the sharp features at low binding energy. Both the raw data (error bars) and deconvoluted data (solid line) are shown. The dotted line is theoretical estimate of the intensity as discussed in the text. The calculated energy positions of each orbital and their degeneracy are indicated by lines at the corresponding binding energies in the lower panel.

of C allotropes the Fermi level is not easily measured directly, but is known to be close to 5 eV below the experimentally determined vacuum level.

For comparison we give the same plots for polycrystalline graphite[17] and amorphous diamond.[8] All three cases have a main band extending from about 26 eV binding energy to about 10 eV binding energy. An effective mass m^* of 1 describes the dispersion of these bands quite well. This structure is comprised of the σ bands. In the graphite and fullerite cases there is another structure. It extends from about 12 eV to 6 eV binding energy and is usually referred to as the π band. In the case of fullerite the π band is split, i.e., at a given binding energy the momentum density peaks for two values of q. Thus far away from the Fermi level the spectral momentum densities of all three cases are rather similar. Near the Fermi level, the differences are much greater, as one would expect just from the large differences in electrical properties of diamond versus graphite/fullerite.

The electronic structure of graphite is determined mainly by the individual sheets of graphite. Dispersion in the direction perpendicular to the sheets is known to be minimal, as the solid in this direction behaves as a van der Waals solid. Due to the small interaction between the planes, graphite is a layered compound which can be cleaved easily. One could get quite a good description of the experimental data if one would do calculations for just a single two-dimensional sheet.

In C_{60} one would expect the dispersive structure to be mainly due to intermolecular bonding. The intramolecular bonding is again the van der Waals type, and is weak as is evident from the low evaporation temperature of C_{60}. It is therefore a useful approach, at least as a first approximation, to compare the measured structure to the molecular calculations.

According to these calculations the occupied electronic structure of a C_{60} molecule consists of 32 orbitals, many of them degenerate. In Fig. 4 we show an experimental momentum-integrated energy spectrum. Clearly we see some structure in the spectra that is due to the discrete orbitals, especially at low binding energy. Many levels are not resolved. The intensity in the measured spectra (error bars) seems to extend to larger binding energies than the calculations. This is at least in part due to energy losses caused by, e.g., plasmon creation by any of the three particles (incoming and outgoing ones) involved. We have tried to correct for these events by an approximate energy deconvolution procedure, using a plasmon of about 25 eV and adjusting the deconvolution in such a way that the measured intensity is zero at large binding energies.[18] The extension of the measured spectra after deconvolution (solid line) agrees quite well with the range of the calculated orbital energies of the calculated orbitals.

In the lower panel of Fig. 4 we show the calculated energy positions of each orbital. The height of each plotted peak is proportional to its degeneracy. The calculations were shifted in energy so that the outermost level lines up with the shoulder at the low-binding-energy side of the spectrum. This relatively small shift ($\simeq 1.7$ eV) is due to a difference in the zero level in the experiment on solid C_{60} and the calculations for an isolated molecule.[19]

At low binding energies the peak structure resembles the distribution of the discrete levels in the molecular C_{60} calculations. At larger binding energy the separation of the different levels is not so clearly resolved, probably as a consequence of the larger intrinsic energy broadening of these levels due to lifetime effects. Similar observations, but with much better energy resolution, were made from photoemission data (see, e.g., Ref. 20).

Using a linear integration of the calculated orbitals over the same momentum range as the experiment we get a theoretical estimate of the measured spectrum after deconvolution for inelastic multiple scattering. The theoretical estimate was broadened by a Gaussian of 1 eV full width half maximum to mimic the energy resolution of the apparatus. This estimate is given as a dotted line in Fig. 4. At small binding energy the measured structures are reproduced qualitatively, but at larger binding energy the measured structure appears to be smeared out, again probably due to lifetime broadening.

The real forte of EMS is that we cannot only measure energy distribution curves, but also resolve the electron momenta. Rather than plotting energy densities integrated over different momentum intervals it is easier to compare the calculated shape of the measured orbitals with the experiment if we plot measured momentum distributions as a function of binding energy. This is done in Fig. 5, which should be compared to Fig. 2. All momentum plots in Fig. 5 have the same normalization constant, i.e., comparing the intensity at dif-

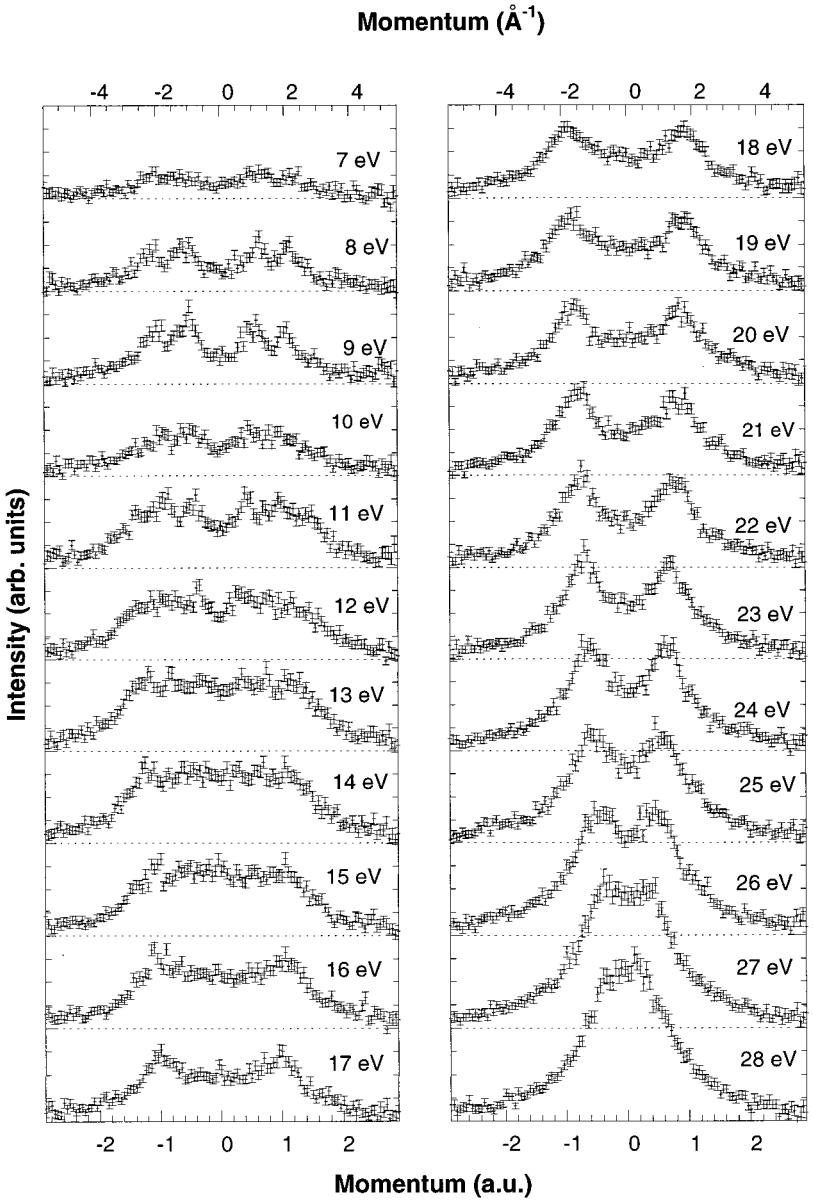

FIG. 5. The measured momentum plots at different binding energies, as indicated. There is quite a continuous shift of the peaks in the momentum distribution with energy, in a way typical for solids.

ferent binding energies is meaningful. In Fig. 2 the momentum densities are for a single orbital, so that in order to obtain the momentum densities in C_{60} the plots have to be multiplied by the indicated degeneracy. Just as in the calculation we have at large binding energy ($\simeq$28 eV relative to the vacuum level) maximum intensity at zero momentum, and for decreasing binding energy the momentum value with maximum intensity increases gradually to larger values. The evolution of the peak position is very similar to the calculated one. In the calculations the intensity at zero momentum drops off to a negligible level with decreasing binding energies, whereas in the measurement the intensity at zero momentum does remain significant. This effect has been understood to be a consequence of additional elastic scattering of one of the electrons involved.[9]

Around 16 eV the minimum between the two peaks disappears. It is at this energy that the π band starts contributing to the intensity. The distribution has a fairly flat plateau around zero momentum for binding energies around 13 eV. It is in the 7–12 eV region that all kinds of distinct features develop. Thus near the Fermi level the structures are sharpest, both in the energy plots and momentum plots.

V. DISCUSSION

Electron-momentum spectroscopy has been applied to atoms, molecules,[7] and solids.[21,22] In a sense the present study is a hybrid. A C_{60} molecule is so big that we can describe it either as a ''small solid'' or a ''big molecule.'' Although we observe in our spectra clear evidence of discrete orbitals, it is also clear that there is a trend toward band structure in the energy-momentum relationship. So it is a nice example to see how the description of the electronic structure of solids and molecules merge for this intermediate case. Small clusters have been studied extensively in literature because of their peculiar structural and electronic properties.[23,24]

We have explored this intermediate behavior with calculations of the momentum density of linear hydrogen chains of different length.[21] A C_{60} molecule is a three-dimensional example of these intermediate cases. In this discussion we

present a simplified model of a C_{60} molecule that gives us an intuitive picture of the relationship between the large numbers of different orbitals. We use the classification of orbitals as proposed by Trouillier and Martin.[16] They described the potential in first approximation as an attractive, spherically symmetric well. The bottom of the well is at the radius of the C_{60} molecule, i.e., 3.55 Å ($\simeq$6.7 a.u.). They estimated the width of the well to be about 3 Å. The solutions of the Schrödinger equation in a spherically symmetric well can be written as the product of a radial function and a spherical harmonic Y_{lm}. The deviations from spherical symmetry can be treated as a perturbation. Only potentials with a symmetry consistent with the icosahedral point group of C_{60} can contribute. This means that perturbations with $l=6$ and $l=10$ contribute. (Trouillier and Martin also considered contributions of the crystal field of the solid, which has tetrahedral symmetry. We neglect these small contributions here.)

Troullier and Martin first calculated the electronic structure of C_{60}, and subsequently analyzed the resulting orbitals in terms of l. In Fig. 2 we indicate their assignments of the different orbitals. The $l=3$ level is the first level that splits due to the icosahedral field contribution with $l=6$. Troullier and Martin did not calculate the momentum densities, but the densities derived from our calculations are in surprisingly good agreement with their simple model. In particular all orbitals that correspond to the same angular momentum have a very similar momentum distribution. Also as angular momentum increases, the momentum value for maximum intensity slowly moves to larger values. In fact for C_{60} we can expect the σ bonding orbitals to be located mainly at the periphery of the molecule, i.e., at a radius r of 6.7 a.u. Then the relation between momentum and angular momentum is simply $l=|\mathbf{p}\times\mathbf{r}|$, thus, if the main momentum component is tangential to the radius, then $p\simeq l/r$. Indeed this simple model predicts the maxima of the momentum orbitals within about 15%.

The energy (in eV) of a given level would be given in first approximation as

$$\varepsilon_l=\varepsilon_0+\frac{l^2}{2m^\star r^2}\times 27.2.$$

With reasonable values ($\varepsilon_0\simeq$25 eV for the σ band, $m^\star\simeq$ close to 1) we get about the right energy of each level (of course we neglect the splitting due to the icosahedral fields in this approximation).

The second type of orbitals, forming the ''π band,'' can be described in a similar way. However these orbitals have an approximate spherical nodal surface at a radius of 3.55 Å, the molecular radius. Therefore this is not a natural choice of the radius of the π charge cloud on this molecule. A more logical choice is to use two different radii, one corresponding to the maximum density of the π charge cloud inside the sphere, and one outside the sphere. A reasonable choice for these parameters ($r_{\text{inner}}=2.55$ Å, $r_{\text{outer}}=4.55$ Å) leads to the right prediction of the peak positions of the double-peaked structure for these orbitals.

Now let us focus once more on the measured momentum plots. In Fig. 6 we show the momentum plots in the energy range corresponding to the top of the valence band. In order to improve the statistics the spectra were folded around zero

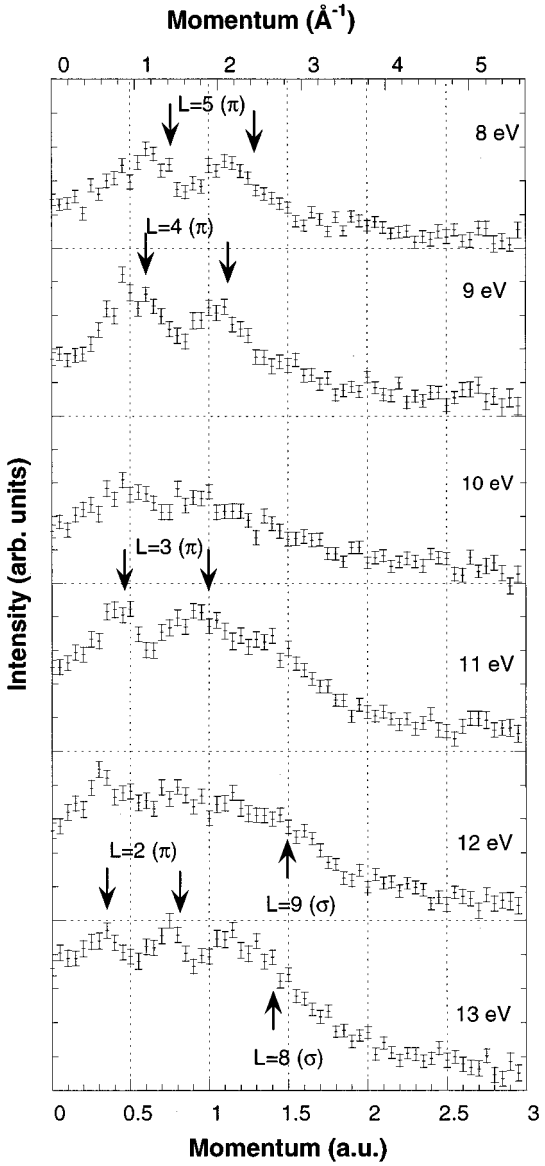

FIG. 6. Details of the momentum distribution at small binding energies. The arrows indicate the calculated peak positions for the different levels as displayed in Fig. 4.

momentum, their symmetry axis. From the alignment of the first shoulder with the HOMO level in the calculations we know that the offset between the zero of the calculations and the measured one is about 2 eV. Now we can associate the expected peak positions, as found from the calculation for each of the angular momentum values, with the measured peak position. We indicate with arrows the expected positions at the appropriate energies. As the HOMO level is not quite resolved we expect the intensity at 8 eV binding energy to be the sum of the $l=5$ and $l=4$ orbitals and indeed the peak position is found close to the average of the momentum values with $l=5$ and $l=4$. The 10 eV plot corresponds with the valley between the $l=4$ and $l=3$ levels at $\simeq$9 eV and $\simeq$11 eV, respectively. Generally the agreement between experiment and calculations is quite good.

There is one thing in the calculation that the measurement does not reproduce. Both $l=0$ orbitals show very large momentum densities at zero momentum (see Fig. 2), so one

would expect very pronounced sharp peaks in the measured momentum densities at these positions. This is not observedWe point out that the $l=0$ level is nondegenerate, whereas most of the other levels are threefold, fourfold, and fivefold . degenerate, a fact that is not included in the height of the theoretical densities in Fig. 2. This still does not explain the absence of clear peaks in the measured densities.

One explanation could be that we measure momentum along a line that, due to some kind of alignment problem, misses zero momentum. We changed the slow electron detector position, as well as the energy of the incoming and fast electron relative to the slow one. In this way we can measure along lines in momentum space that are shifted slightly relative to the original one. No sign of strong peaks was found.

The other explanation could be that the peaks are not there, at least not in solid C_{60}. The full width at half maximum of these peaks is about 0.2 a.u. Thus the dimension of the charge cloud in coordinate space is of the order of 5 a.u. (2.5 Å). This is of the order of the intramolecular distance, so overlap effects may be important here. For the other levels the momentum values are mainly determined by the tangential component, which would explain why these are less sensitive to the ''radial'' overlap.

VI. CONCLUSION

We have measured the spectral momentum density of solid C_{60} and compared it to calculations of the electronic structure of a single molecule. Generally good agreement was found. Qualitative understanding is obtained if one models the C_{60} molecule as a spherical well. The orbitals can then be classified in terms of angular momentum. This quantum number determines, in first approximation, the momentum value for which the density is maximum, and the binding energy of the orbitals. For the π band there is a double structure for the orbitals in momentum space which within this model is a simple consequence of curvature of the carbon planes. Generally it turns out that C_{60} is a fascinating case which, within our experimental resolution, displays both characteristics of a molecule (discrete levels) and a solid (dispersion).

ACKNOWLEDGMENTS

This research was funded by a grant of the Australian Research Council. M.T.M. wishes to thank Professor J. Bernholc for providing the C_{60} input coordinates. The computations were performed on CSIRO Supercomputing Facility CRAY Y-MP4/464 in Melbourne.

*Present address: Atomic and Molecular Physics Laboratory, Research School of Physical Sciences and Engineering, the Australian National University, Canberra 0200, Australia.

[1] J. Robertson, Prog. Solid State Chem. **21**, 199 (1991).
[2] M. S. Dresselhaus, G. Dresselhaus, and P. C. Ecklund, J. Mater. Res. **8**, 2054 (1993).
[3] M. Vos, Z. Fang, S. Canney, A. Kheifets, I. E. McCarthy, and E. Weigold, Phys. Rev. B (to be published).
[4] M. Vos, P. Storer, S. A. Canney, A. S. Kheifets, I. E. McCarthy, and E. Weigold, Phys. Rev. B **50**, 5635 (1994).
[5] P. Storer, Y. Q. Cai, S. A. Canney, S. A. C. Clark, A. S. Kheifets, I. E. McCarthy, S. Utteridge, M. Vos, and E. Weigold, J. Phys. D **28**, 2340 (1995).
[6] M. Vos, P. J. Storer, Y. Q. Cai, I. E. McCarthy, and E. Weigold, Phys. Rev. B **51**, 1866 (1995).
[7] I. E. McCarthy and E. Weigold, Rep. Prog. Phys. **54**, 789 (1991).
[8] P. Storer, R. S. Caprari, S. A. C. Clark, M. Vos, and E. Weigold, Rev. Sci. Instrum. **65**, 2214 (1994).
[9] M. Vos and M. Bottema, Phys. Rev. B **54**, 5946 (1996).
[10] M. Vos, P. J. Storer, Y. Q. Cai, A. S. Kheifets, I. E. McCarthy, and E. Weigold, J. Phys., Condens. Matter. **7**, 279 (1995).
[11] S. Canney, M. Vos, A. S. Kheifets, N. Clisby, I. E. McCarthy, and E. Weigold, J. Phys. Condens. Matter. **9**, 1931 (1997).
[12] J. Andzelm and E. Wimmer, J. Chem. Phys. **96**, 1290 (1992).
[13] A. Komornicki and G. Fitzgerald, J. Chem. Phys. **98**, 1398 (1993).
[14] *UniChem*^{TM} Chemistry Codes, APG-5505 3.0, Cray Research, Inc., pp. 145–190.
[15] Q. Zhang, J.-Y. Yi, and J. Bernholc, Phys. Rev. Lett. **66**, 2633 (1991).
[16] N. Troullier and J. L. Martin, Phys. Rev. B **46**, 1754 (1992).
[17] A. S. Kheifets and M. Vos, J. Phys., Condens. Matter. **7**, 3895 (1995).
[18] R. Jones and A. L. Ritter, J. Electron Spectrosc. Relat. Phenom. **40**, 285 (1986).
[19] J. W. Gadzuk, Phys. Rev. B **14**, 2267 (1976).
[20] J. H. Weaver, J. L. Martins, T. Komeda, Y. Chen, T. R. Ohno, G. H. Kroll, N. Troullier, R. E. Haufner, and R. E. Smalley, Phys. Rev. Lett. **66**, 1741 (1991).
[21] M. Vos and I. E. McCarthy, Rev. Mod. Phys. **67**, 713 (1995).
[22] J. R. Dennison and A. L. Ritter, J. Electron Spectrosc. Relat. Phenom. **77**, 99 (1996).
[23] *Physics and Chemistry of Small Clusters*, edited by P. Jena, B. K. Rao, and S. N. Khanna (Plenum, New York, 1987).
[24] W. A. de Heer, W. D. Knight, M. Y. Chou, M. L. Cohen, Solid State Phys. **40**, 93 (1987).